

3-D simulation of gases transport under condition of inert gas injection into goaf

Mao-Xi Liu, Guo-Qing Shi, Zhixiong Guo, Yan-Ming Wang & Li-Yang Ma

Heat and Mass Transfer
Wärme- und Stoffübertragung

ISSN 0947-7411
Volume 52
Number 12

Heat Mass Transfer (2016) 52:2723–2734
DOI 10.1007/s00231-016-1775-8

231 Research Journal

Heat and Mass Transfer

Wärme- und Stoffübertragung

52
12

 Springer

Volume 52 • Number 12 • December 2016

ORIGINALS

Experimental investigation of head resistance reduction in bubbly Couette-Taylor flow
R. Maryami · M. Javadpoor · S. Farahat 2603

Performance improvement of wire-bonded mesh screen flat heat pipe using water-based nanofluid
P.-Y. Wang · Y.-J. Chen · Z.-H. Liu 2609

A new optimization approach for shell and tube heat exchangers by using electromagnetism-like algorithm (EM)
A.M. Abel · I.A. Abel · H.Sh. Majidi · A.N. Al-Shamani · K. Sopian 2613

CFD modeling using PDF approach for investigating the flame length in rotary kilns
H.E. Elatar · E. Specht · A. Fouad · A.S. Bin-Mahfouz 2635

Experimental study of water desorption isotherms and thin-layer convective drying kinetics of bay laurel leaves
T. Ghimmi · L. Hassini · M. Bagane 2649

Experimental determination of thermal properties of alluvial soil
N.G. Kulbari · U.V. Bhandarkar · R.P. Purankar · A.B. Rao 2661

Simulation and experimental validation of droplet dynamics in microchannels of PEM fuel cells
M. Ashrafi · M. Shams · A. Bozorgnezhad · G. Ahmadi 2671

Effect of bend separation distance on the mass transfer in back-to-back pipe bends arranged in a 180° configuration
X. Chen · T.L. Lee · D. Ewing · C.Y. Chung 2687

Determination of the drying and rehydration kinetics of freeze dried kiwi (*Actinidia deliciosa*) slices
K. Ergün · G. Çalışkan · S.N. Dirim 2697

Experimental and numerical investigation on the performance of an internally cooled dehumidifier
O.E. Turgut · M.T. Çoban 2707

3-D simulation of gases transport under condition of inert gas injection into goaf
M.-X. Liu · G.-Q. Shi · Z. Guo · Y.-M. Wang · L.-Y. Ma 2723

SiO₂ nanofluid planar jet impingement cooling on a convex heated plate
N. Asghari Lafajani · M. Ebrahimi Bidhendi · M. Ahsjace 2735

Experimental investigation on the thermal performance of heat storage walls coupled with active solar systems
C. Zhao · S. You · C. Zhu · W. Yu 2747

The influence of tip clearance and Prandtl number on turbulent forced convection heat transfer of rectangular fins
H.-K. Park · B.-J. Chung 2759

Boiling heat transfer enhancement of nanofluids on a smooth surface with agitation
X. Kong · R. Qi · J. Wei · W. Li · J. Ding · Y. Zhang 2769

Assessment of zero-equation SGS models for simulating indoor environment
I. Taghnia · M.M. Rahman · T.K.T. Tee 2781

Comparative study of solar air heater performance with various shapes and configurations of obstacles
K. Kulbari · K.-Y. Kim 2795

Study on effective thermal conductivity of silicone/phosphor composite and its size effect by Lattice Boltzmann method
L. Li · H. Zheng · C. Yuan · R. Hu · X. Luo 2813

(Continuation on cover page VIII)

S2 (12) 2593–2912 (2016)

Your article is protected by copyright and all rights are held exclusively by Springer-Verlag Berlin Heidelberg. This e-offprint is for personal use only and shall not be self-archived in electronic repositories. If you wish to self-archive your article, please use the accepted manuscript version for posting on your own website. You may further deposit the accepted manuscript version in any repository, provided it is only made publicly available 12 months after official publication or later and provided acknowledgement is given to the original source of publication and a link is inserted to the published article on Springer's website. The link must be accompanied by the following text: "The final publication is available at link.springer.com".



3-D simulation of gases transport under condition of inert gas injection into goaf

Mao-Xi Liu¹ · Guo-Qing Shi^{1,2} · Zhixiong Guo² · Yan-Ming Wang¹ · Li-Yang Ma¹Received: 16 September 2015 / Accepted: 10 February 2016 / Published online: 20 February 2016
© Springer-Verlag Berlin Heidelberg 2016

Abstract To prevent coal spontaneous combustion in mines, it is paramount to understand O₂ gas distribution under condition of inert gas injection into goaf. In this study, the goaf was modeled as a 3-D porous medium based on stress distribution. The variation of O₂ distribution influenced by CO₂ or N₂ injection was simulated based on the multi-component gases transport and the Navier–Stokes equations using Fluent. The numerical results without inert gas injection were compared with field measurements to validate the simulation model. Simulations with inert gas injection show that CO₂ gas mainly accumulates at the goaf floor level; however, a notable portion of N₂ gas moves upward. The evolution of the spontaneous combustion risky zone with continuous inert gas injection can be classified into three phases: slow inerting phase, rapid accelerating inerting phase, and stable inerting phase. The asphyxia zone with CO₂ injection is about 1.25–2.4 times larger than that with N₂ injection. The efficacy of preventing and putting out mine fires is strongly related with the inert gas injecting position. Ideal injections are located in the oxidation zone or the transitional zone between oxidation zone and heat dissipation zone.

List of symbols

A Pro-factor

a_0	Attenuation rate in the tendency direction
a_1	Attenuation rate in the strike direction
b_0, b_1	Adjusting parameters
C	Mass concentration
D	Diffusivity (m ² s ⁻¹)
E	Activation energy (kJ/mol)
\vec{g}	Vector of gravity (ms ⁻²)
H	Height (m)
K	Coefficient of rock dilatation
$K_{p,\max}$	Initial caving coefficient
$K_{p,\min}$	Coefficient of bulk increase
k	Permeability (m ²)
k_0	Base permeability (m ²)
L	Length (m)
\dot{m}	Mass generation rate (kg/m ³ s)
P	Pressure (N/m ²)
R	Ideal gas constant
S	Source term
T	Temperature (K)
t	Time (s)
\mathbf{u}	Velocity vector
u, v, w	Velocity components (m/s)
W	Width (m)
x, y, z	Spatial coordinates

Greek symbols

α	Reaction constant
ε	Adjusting parameter
ξ	Porosity
μ	Dynamic viscosity [kg/(m s)]
ρ	Density of the gas mixture (kg/m ³)

Subscripts

 i Gas component

✉ Guo-Qing Shi
shiguoqing2001@163.com

Zhixiong Guo
guo@jove.rutgers.edu

¹ College of Safety Engineering, China University of Mine Technology, Xuzhou 221008, Jiangsu, China

² Department of Mechanical and Aerospace Engineering, Rutgers, State University of New Jersey, Piscataway, NJ 08854, USA

1 Introduction

Coal spontaneous combustion is a serious issue that threatens the development of coal industry worldwide [1]. Among China's state-owned collieries, 56 % of the mines have been jeopardized by spontaneous combustion; and the combustion incidents in these mines account for 90–94 % of all coalmine fires [2]. Goaf is one of the most vulnerable places for coal spontaneous combustion.

Spontaneous combustion of coal occurs through a very complex process involving thermal [3], hydraulic [4], chemical and mechanical aspects [5]. Coal oxidation [1, 5] is the root cause of spontaneous combustion. Therefore, spontaneous combustion of coal underground is closely related to the distribution of oxygen gas in goaf [6]. Some researchers believe that there exists a critical O₂ concentration (depending on rank of coal) for supporting coal spontaneous combustion; i.e., if there were no or not enough O₂ gas, coal spontaneous combustion would not happen. Therefore, it is desirable to reduce O₂ concentration in order to prevent coal fire in goaf. To this end, there are two common approaches: one is to reduce air leakage into goaf from workface [7]; and the other is injection of inert gas into goaf to dilute oxygen [8]. The inert gases used in coal goaf are mainly nitrogen [9] and carbon dioxide [10].

However, little is known of critical parameters such as the optimal and economical positions and time in injecting CO₂ or N₂ gas. The influence scope with injection of CO₂ or N₂ in goaf is quantitatively undetermined. Meanwhile, little is known about the difference of the effects on the coal spontaneous combustion area and the O₂ concentration during injection of inert gas. As a matter of fact, improper position of injection may increase the likelihood of mine fires.

Since goaf is human inaccessible, it is hardly possible to collect sufficient field data in goaf at the current experimental conditions. Instead, CFD modeling approach was commonly adopted to study these issues [1, 8, 9, 11]. CFD simulation is a promising approach to gain deep insight into the goaf flow field and to analyze temporally and spatially the effects of air leakage from workface or injection of inert gas on O₂ gas distribution. Liang et al. [12] proposed a 2-D porous medium model for goaf and simulated the gas flow field. Li et al. [9] analyzed N₂ gas injection parameters and the airflow field status and O₂ concentration distribution in goaf. Shao et al. [8] presented a steady-state model and estimated the effect of injecting CO₂ gas on oxygen concentration. Zhang et al. [10] revealed some variations of the oxidized zone and the asphyxia zone with injection of CO₂ gas. Che et al. [13] studied the coupling law of mixed gas in 3-D goaf. Yuan and Smith [14] conducted a 3-D simulation of spontaneous heating in a large-scale coal chamber in a forced ventilation system. Nevertheless, very

few studies are available about the difference between CO₂ and N₂ injections into goaf. The O₂ concentration with CO₂ or N₂ injection varies as time develops. The relationship between the positions of injection and the efficacy of preventing and putting out mine fires is unclear. More studies are needed to optimize the injection of inert gas.

In this paper, we developed a 3-D CFD model to study gases transport with injection of inert gas into mine goaf. The goaf simulated a field experiment. The coupling between chemical reactions in the coal seam and O₂ gas transport through adjacent rocks was taken into account. The distributions of O₂, CO₂ or N₂ gases in the goaf were obtained. We also discussed the inerting effect due to the location of perfusion pipeline's exports. The results were used to evaluate the hazard of coal spontaneous combustion in specific areas of the goaf under condition of inert gas injection. These data would be useful for prevention of coal spontaneous combustion and lay a foundation on the fulfillment of inert gas injection for coal fire controlling.

2 Field measurement

Figure 1 shows the schematic diagram of our field experiment conducted in 3418 workface in Liangbaosi coal mine in China, which is a complex mechanical coal mining workface with fully mechanized top coal caving technology. The mining elevation varies from -607.1 to -871.6 m level. The length and width of the coal seam are 2113 and 100 m, respectively. The slope angle of the coal seam varies from 4° to 15°, with an average angle of 9°. The thickness of the coal seam is between 1.3 and 9.2 m, with an average thickness of 6.35 m. The air quantity of mining workface is 768 m³/min, and the ventilation system is a "U" type model.

To investigate the effect of proactive inertization in goaf, it is very important to characterize the initial O₂ gas pattern. This involves a detailed monitoring of the gas distribution behind the workface. To this end, four gas sampling

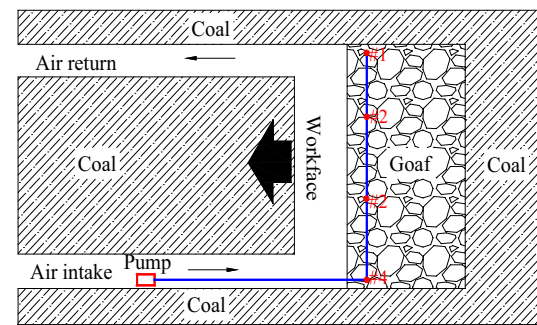


Fig. 1 Schematic diagram of field experiment

pipelines were installed in the goaf and their entry positions are marked as #1 to #4 in Fig. 1. The distance of the four measuring pipelines from the air return-side is about 1, 34, 67 and 99 m, respectively. We collected the gas from the measuring pipelines through a bundle pipeline system. To avoid the destruction of the bundle pipeline by caving rocks, steel pipes were used to protect the bundle pipelines. The gas samples were analyzed using a KSS-200 chromatograph. This device can be used to analyze the following gases (molar concentration ranges): O₂ (0–25 %); N₂ (70–98 %); CO, C₂H₄, C₂H₆, and C₂H₂ (0–50 %); and CH₄ and CO₂ (0–80 %). It has an accuracy ≤ 1 ppm and a relative error ≤ 1.5 %.

3 Mathematical models

Figure 2 shows the goaf model employed in the present numerical simulation, adapted from the conditions in field measurement described above. The model goaf is 150 m long, 100 m wide, and 40 m high. The coal seam angle is 0° and the strike angle is 9°. The cross section size of both the workface and laneway is 4 m × 4 m. The length of the laneway is 16 m. The coordinate origin is located at the junction of the workface and the goaf on the intake-side. Inert gas injection was considered from one of the six injection ports from either the air intake or return side and located in the heat dissipation zone ($l_1 = 12$ m), the oxidation zone ($l_3 = 60$ m), and the transitional zone ($l_2 = 36$ m) between the heat dissipation zone and the oxidation zone, respectively.

The air leakage mainly consisting of N₂ and O₂ gases seeps into the goaf from the workface under the mine ventilation pressure. Meanwhile, residual coal desorbs methane and it is also oxidized by O₂ slowly in the goaf. Spontaneous combustion of coal occurs when sufficient O₂ gas is available and the heat that is produced by the low-temperature oxidation reaction of coal with O₂ is not adequately dissipated by conduction or convection, resulting in a net temperature increase in the coal mass. Under conditions

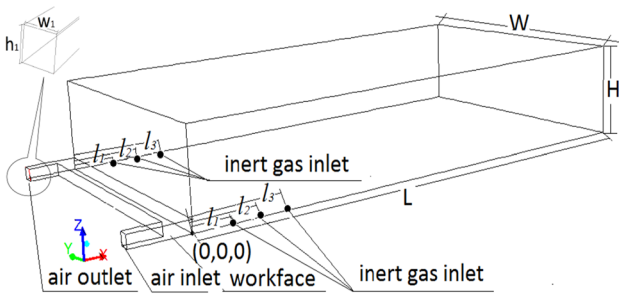


Fig. 2 The goaf model used in simulation

that favor a high heating rate, the coal attains thermal runaway and then a fire ensues.

Coal desorbs methane and its self-ignition also consumes O₂, leading to variance of gases distribution. The species mass conservation equation under incompressible flow condition is:

$$\xi \frac{\partial(\rho C_i)}{\partial t} + \rho \nabla \cdot (C_i \mathbf{u}) = \xi \rho \nabla \cdot [D_i \nabla(C_i)] + S_i \quad i = 1, 2, 3, 4 \quad (1)$$

where ρ is the density of the gas mixture, C_i and D_i are the mass concentration and diffusion coefficient of the gas species, ξ is porosity, S_i is the source term, t represents time, \mathbf{u} is velocity vector. Subscripts 1 to 4 represent N₂, CO₂, O₂ and CH₄ gas in order. In the present study, $S_1 = S_2 = 0$ everywhere, $S_3 = S_4 = 0$ in the laneway, and in the goaf S_3 and S_4 are described by [14]:

$$S_3 = -AC_3^\alpha e^{-\frac{E}{RT}} \quad (2)$$

$$S_4 = \dot{m}_4 \quad (3)$$

where A is the pro-factor, decided by the species of coal and the test methods; α is a constant, varying from 0.5 to 1.0; E is the activation energy, varying between 12 and 95 kJ/mol depending on coal species; R is the ideal gas constant; T is the absolute temperature; and \dot{m}_4 is the CH₄ gas mass generation rate per unit volume measured by field experiment.

We assume that the mine goaf is an isotropic porous medium. Since the gas mixture could be assumed as Newtonian fluid, the vector form of the momentum conservation equations in the porous goaf is [13, 15]

$$\frac{\rho}{\xi} \left(\frac{\partial \mathbf{u}}{\partial t} + (\mathbf{u} \cdot \nabla) \mathbf{u} \right) = -\nabla \cdot P + \frac{\mu}{\xi} \cdot (\nabla^2 \mathbf{u}) + \rho \vec{g} - \frac{\mu}{k} \mathbf{u} \quad (4)$$

where P is the pressure, μ is the dynamic viscosity of the gas mixture, \vec{g} is the vector of gravity, and k is the permeability of the goaf.

The pressure gradient and concentration gradient drive the gases seep into the goaf. When the gas transfers in goaf, it is hindered with the viscous resistance and inertia resistance. All these factors are highly associated with the permeability distribution of the goaf. Qian and Li [16] illustrated a function between the goaf permeability and the surrounding rock stress, which is an exponential distribution at the strike direction. According to the Carman–Konzeny equation, permeability can be described as:

$$k = \frac{k_0}{0.241} \cdot \frac{\xi^3}{(1 - \xi)^2} \quad (5)$$

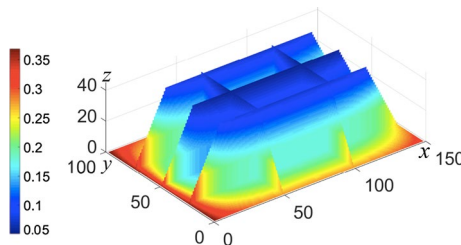


Fig. 3 3-D mapping of goaf porosity used in simulation

where k_0 is the base permeability of the broken rock at the maximum porosity and it was taken as $1 \times 10^{-3} \text{ m}^2$, which places it the “open jointed rock” range according to Hoek and Bray [17].

Overlying rocks tend to subside because of overburden pressure and mechanical failure induced by volume losses of coal seam. Since both the hydraulic system and the surrounding rock support the overlying rocks, the porosity of goaf decreases initially and then increases at the strike direction. In general, the porosity is smaller in the middle of the goaf because the caving rock is in compaction; and it is larger in the zone near the intake and return airways. The porosity also decreases with the z -level rising. Some 2-D goaf porosity models were established in previous studies [18–22]. In this paper, we optimized the porosity model and introduced a 3-D porosity model as

$$\xi = \left\{ 1 - \left[K_{p,\min} + (K_{p,\max} - K_{p,\min}) \times \exp[-a_1(y + b_1)] \left(1 - e^{-\varepsilon a_0(x + b_0)} \right) \right] \right\}^{-1} \times \left(1 - \frac{z}{H} \right) \quad (6)$$

where $K_{p,\max}$ is the initial caving coefficient of bulk increase and its value is 1.6; $K_{p,\min}$ is the coefficient of bulk increase in compaction and its value is 1.1; a_0 and a_1 are the attenuation rate in the tendency and strike direction, respectively, and their values are 0.0368 and 0.268; ε_1 is the adjusting parameter and its value is 0.233 [19]; b_0 and b_1 are the adjusting parameters in the strike direction and at the tendency, and their values are 0.8 and 15; H is the height of goaf. The porosity distribution for the goaf in the present study is shown in Fig. 3.

The boundary conditions for the simulation model were established based on the field experimental conditions and are described below. Compared with goaf, the porosity and permeability of coal seam around the goaf are very small, so it could be assumed as solid wall. Thus, at all boundary walls of the goaf and the laneway:

$$u = 0, \quad C_i = 0 \quad (7)$$

At the fresh air inlet of the laneway:

$$\begin{aligned} &C_1 = 0.77 \\ &u = v_{air} \quad C_3 = 0.23 \\ &v = w = 0 \quad C_2 = C_4 = 0 \end{aligned} \quad (8)$$

At the air outlet of the laneway:

$$P = p_0 \quad (9)$$

In the case with N_2 injection, the injection inlet:

$$\begin{aligned} &u = v_{N_2} \quad C_1 = 1 \\ &v = w = 0 \quad C_2 = C_3 = C_4 = 0 \end{aligned} \quad (10)$$

In the case with CO_2 injection, the injection inlet:

$$\begin{aligned} &u = v_{CO_2} \quad C_2 = 1 \\ &v = w = 0 \quad C_1 = C_3 = C_4 = 0 \end{aligned} \quad (11)$$

In Which, v_{air} is the air velocity calculated by the airflow rate and cross section size of laneway. v_{N_2} and v_{CO_2} are the velocities of inert N_2 and CO_2 gas injection, respectively, calculated by injection rate and cross section size of the injection port. p_0 is the pressure around the mine goaf. The return airway is set as a free outflow condition.

The simulation model was meshed using unstructured grids. Several mesh sizes were considered. We found that a grid system containing 595,854 nodes and 3,402,152 elements could give satisfactory convergent results and this

grid size was adopted for simulations thereafter. For the solution to converge easily, the mesh around the inert gas inlet was refined.

The commercial software package, FLUENT (ANSYS 14.5), was used in the present simulations. The species transport model is actually a built-in model in FLUENT. Meanwhile, the secondary development of FLUENT was carried out with User Defined Function (UDF). The porosity profile and inertia resistance were defined with “DEFINE_PROFIL”. The oxygen consumption rate was defined with “DEFINE_SOURCE”. Then the UDF was combined with FLUENT. The convergence of all the variables was that their residuals are $< 10^{-3}$ [15, 23].

4 Results and discussion

Figure 4 displays the measured O_2 gas molar concentration distributions at the four measuring pipelines in the field

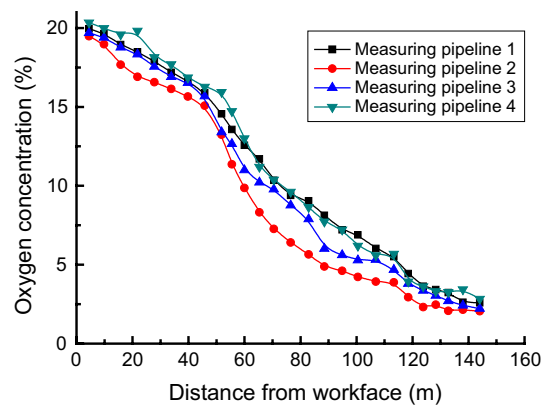


Fig. 4 O_2 distributions from field measurement

experiment. There was no injection of inert gas. From Fig. 4, it is seen that the O_2 gas concentration decreases as distance (x value) increases. Since the air leakage flows into the goaf under the mine ventilation pressure, the farther the location is away from the workface, the weaker the air leakage flow is. Meanwhile, the residual coal desorbs methane and coal oxidation consumes oxygen; all these factors decrease O_2 concentration with increasing x distance. It is observed that O_2 concentration is a little bit higher on air return-side (measuring pipeline #1) and intake-side (measuring pipeline

#4) than the middle parts (measuring pipelines #2 and #3). The reason is that there are substantial structural fractures in the caving rocks. So the porosity is larger and the vicious resistance is smaller in the area near the four boundaries of the goaf. And the air quantity of the air leakage ingress on both sides is larger. In the middle of the goaf, the overlying rocks are in the cantilever beam structure. The overlying rocks would cave in a short time period and then the caving rocks would be compacted by mine pressure. The vacuity between rocks is little, which hinders the air seepage in the goaf. Further, the chemical reaction also consumes oxygen, resulting in further O_2 dips in the goaf middle.

Usually the goaf can be demarcated into three zones according to O_2 concentration level: heat dissipation zone ($O_2 > 15\%$), oxidation zone ($15\% > O_2 > 5\%$) and the asphyxia zone ($O_2 < 5\%$). In the asphyxia zone, especially when O_2 concentration is below the level of 3 %, coal oxidation stops [24, 25]. Because the flow of air leakage is very weak, no enough oxygen is available for constant coal oxidation and spontaneous combustion wouldn't happen. That is to say, if the asphyxia zone were larger, the risk of coal spontaneous combustion would be lower. Oxidation zone is the area where the coal spontaneous combustion mostly happens based on the data we obtained from field experiment. The scope of the oxidation zone is from 36–52 to 90–114 m behind the workface.

Fig. 5 Comparison of O_2 molar concentration distributions between field measurements and simulations. **a** Measuring pipeline 1, **b** measuring pipeline 2, **c** measuring pipeline 3, **d** measuring pipeline 4

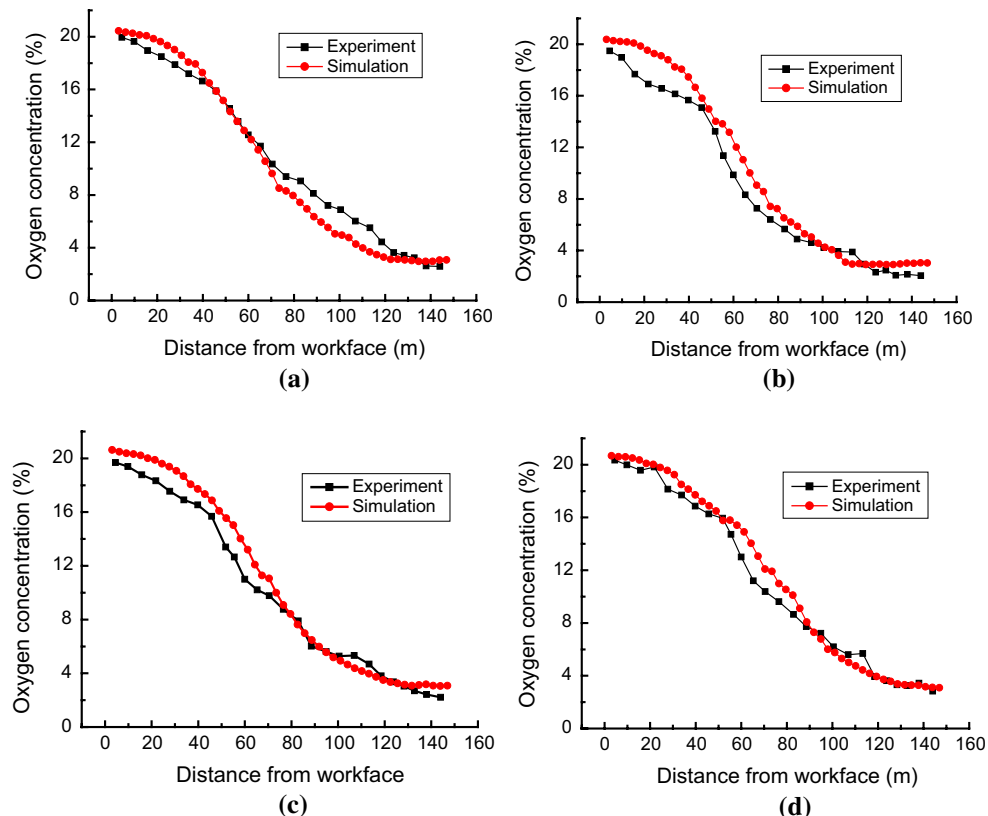


Fig. 6 Cloud pictures of CO₂ molar concentration at different z-levels with CO₂ injection 36 m behind the workface

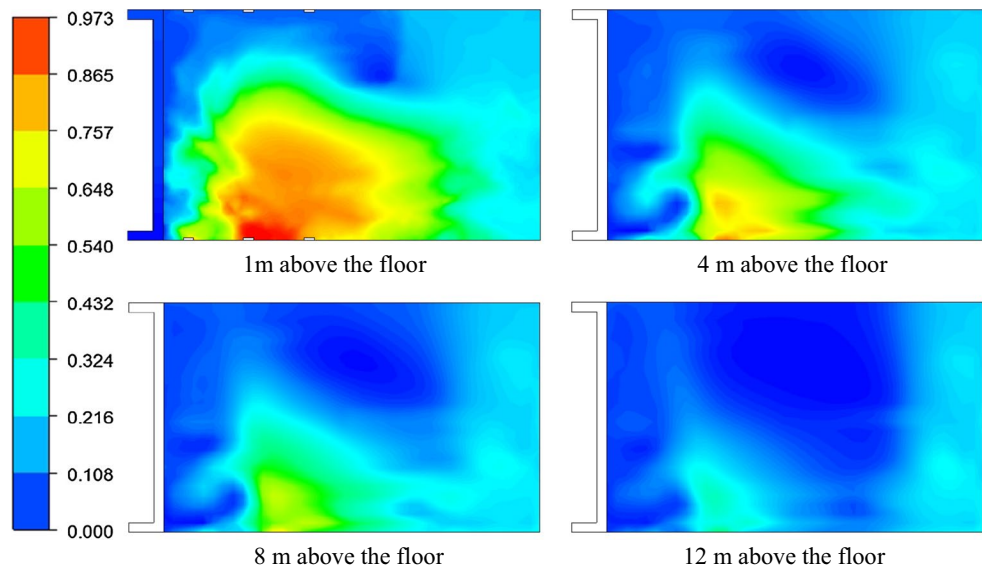
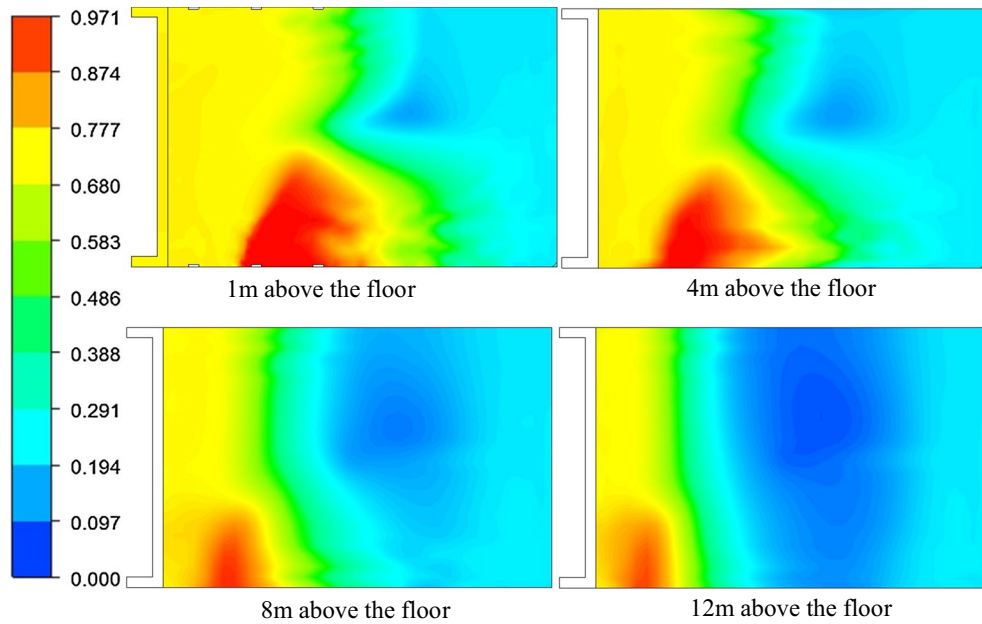


Fig. 7 Cloud pictures of N₂ molar concentration at different z-levels with N₂ injection from 36 m behind the workface



To validate our simulation model, we compared the simulation results without inert gas injection with the field measurement data in Fig. 5, in which the comparison is shown for each measuring pipeline. The simulation was set in similar conditions as in the field experiment. For example, the airflow rate is at 768 m³/min and the O₂ molar concentration in the airflow is 20.95 % (equals to mass concentration at 23 %). It is found that the simulation results have a good consistency with the experimental data. The changing trend of the simulation data is the same as the experimental measurement.

The validated numerical model is then used for extensive parametric studies involving inert gas injection, for

which experimental study is difficult. For all the simulations thereafter, we kept the same airflow conditions specified before. The volume flow rate of CO₂ or N₂ injection is 720 m³/h.

Figures 6 and 7 show the cloud pictures of CO₂ and N₂ molar concentrations, respectively, with corresponding inert gas injection. Figure 8 compares O₂ molar concentration distributions in sections 1, 10 and 20 m away from the intake-side with or without inert gas injection. From Fig. 6, it is found that CO₂ concentration reduces as the goaf z-level rises. The reason is that CO₂ gas is heavier than other gases. Therefore, CO₂ accumulated in the zone near the goaf floor. The region where CO₂ concentration

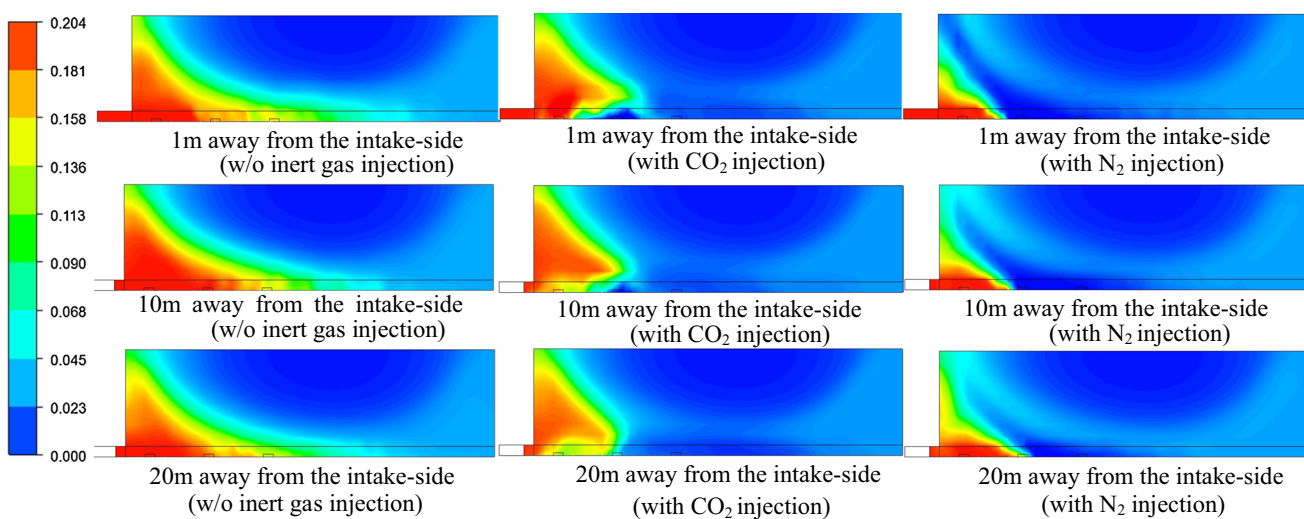


Fig. 8 O₂ distributions in x-z cross-sections of y = 1, 10 and 20 m, respectively

is above 10 % is about 49.6–67.2 % of the whole goaf volume. Analysis of the results in Fig. 8 shows that CO₂ injection has a major influence on O₂ distribution from the floor ($z = 0$) of the goaf up to 12 m above the floor. Beyond that, CO₂ injection seems to play little role on the O₂ distribution. Meanwhile, CO₂ is difficult to mix with air. It stratifies in the goaf and forms a zone in which O₂ is below 3 % or even no oxygen, decreasing the area of spontaneous combustion zone and the spontaneous combustion dangerousness.

From Fig. 7, it is seen that the location around the N₂ injection entrance has a N₂ concentration >97 %. N₂ concentration is still over 97 % when it is 8–12 m above the floor of the goaf. It indicates that N₂ gas flows up in the goaf. Since the density of N₂ is less than that of the air, the buoyancy has a major influence on the N₂ gas distribution. Analysis of the results in Fig. 8 also shows nitrogen flows to the workforce with rising z . The location where oxidation zone starts is about 32, 26, 16 and 12 m away from to the workforce when $z = 1, 4, 8$ and 12 m, respectively. It is obvious that a portion of nitrogen seeps to the fractured zone and moves to the workforce at the top of the goaf because of the gravity and ventilation pressure, which weakens the dilution effect on the oxygen at the goaf floor.

The accumulation of nitrogen and carbon dioxide is quite different because of their different physicochemical properties. Since the density of CO₂ is 1.5 times as the density of air, CO₂ accumulates usually at the ground level. Therefore, CO₂ injection dilutes the O₂ concentration significantly and decreases the area of the spontaneous combustion zone. Meanwhile, the N₂ dilutes the O₂ around the inert gas injection port zone and a large portion of N₂ diffuses to the fractured zone, which reduces the effect on diluting oxygen.

Figures 9 and 10 show the time development of O₂ molar concentration distribution at the ground level with continuous CO₂ and N₂ injection, respectively. It is found that CO₂ or N₂ injection changes the oxygen distribution of the goaf. Inert gas injection dilutes the oxygen and reduces the oxygen concentration. O₂ concentration in the zone near the inert gas injection position decreases sharply in the first 4 h, and then the area influenced by inert gas becomes larger gradually. The O₂ distribution becomes stable 16 h after.

During the process of inert gas injection, the area of spontaneous combustion dangerous zone (incl. heat dissipation zone and oxidation zone) also reduces, as shown in Fig. 11. Since CO₂ is heavy, injection of CO₂ is more profound in reducing the spontaneous combustion risky zone than N₂ gas. The time evolution of the spontaneous combustion dangerous zone at the ground level can be classified into three phases: Phase I: slow inerting phase ($t < 2$ h); Phase II: rapid accelerating inerting phase ($2 \text{ h} < t < 20$ h); and Phase III: stable inerting phase ($t > 20$ h). In phase I, CO₂ accumulates around the injection port. The area dangerous zone decreases slowly and shows level changes with time. Nitrogen injection showed similar phenomena in this phase. In phase II, CO₂ seeps and drives the gas mixture to diffuse in the goaf, O₂ concentration dips sharply. The area changing rate of the dangerous zone with CO₂ injection shows a negative exponential relationship with time. On the other side, the rate with N₂ injection is smaller because a portion of the nitrogen seeps to the fractured zone. The rate of the dangerous zone with N₂ injection shows a negative linear relationship. CO₂ and N₂ injection would reduce the area of the spontaneous combustion dangerous zone in 12 and 20 h, respectively. Therefore, CO₂ decreases the oxygen concentration and the area of the spontaneous

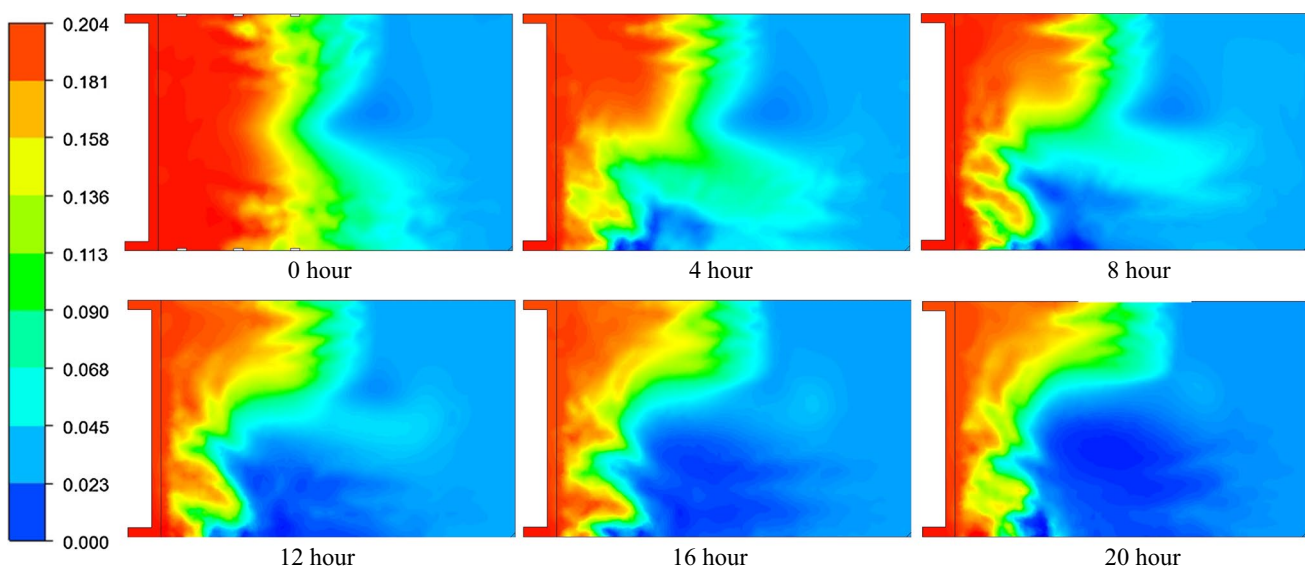


Fig. 9 Time development of O_2 distribution at the goaf floor level with CO_2 injection

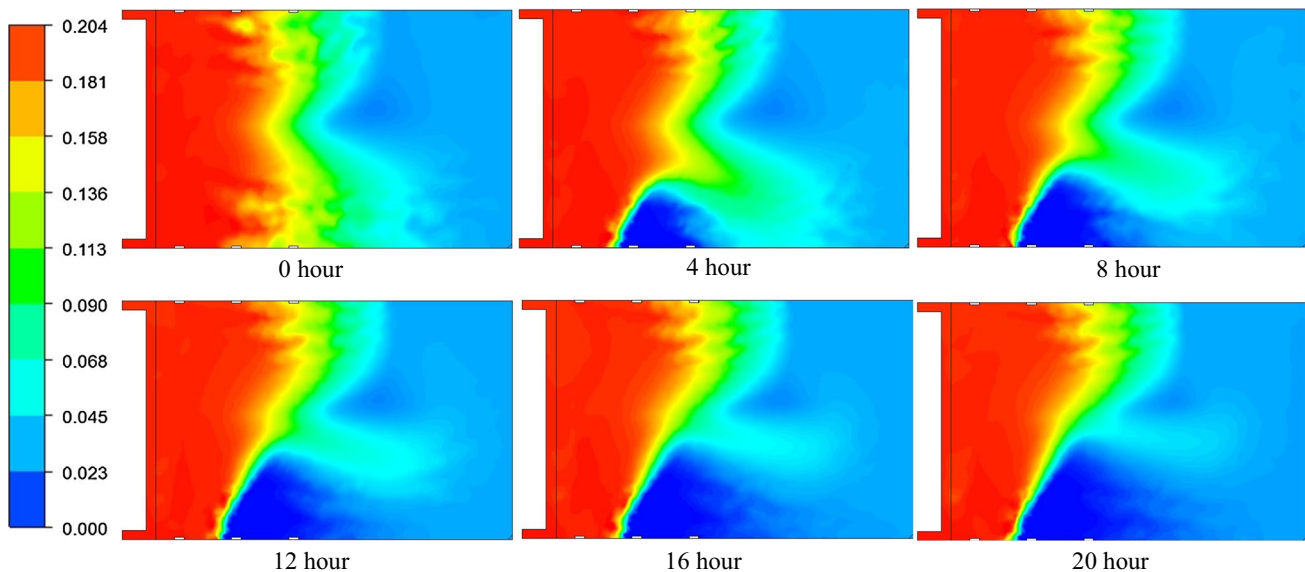


Fig. 10 Time development of O_2 distribution at the goaf floor level with N_2 injection

combustion dangerous zone in a short time, much faster than the injection of nitrogen. In phase III, the injected inert gas reaches a new gas equilibrium with the original gases in the goaf. Spontaneous combustion dangerous zone decreases slowly or keeps steady. Therefore, the time of the slow inserting phase and rapid accelerating inserting phase can be justified as a reasonable time for injecting inert gas.

The location effect of inert gas injection was investigated and shown in Figs. 12 and 13 for CO_2 and N_2 injection, respectively. The injection was considered at 12, 36 and 60 m behind the workface from each the intake-side

or return-side, respectively; altogether there are 6 different locations. From Fig. 12, we can see that when CO_2 injection is located at 12 m behind the workface, the area of the oxidation is not obviously influenced. This is because air-leakage speed is larger when inert gas is injected at 12 m behind the workface. So the air leakage carries away the CO_2 gas to the workface, little inert gas remains in the goaf. Similar patterns can be found with N_2 injection at 12 m behind the workface as shown in Fig. 13.

The effect on O_2 distribution in the goaf is almost same when the inert gas injection location is 36 and 60 m behind

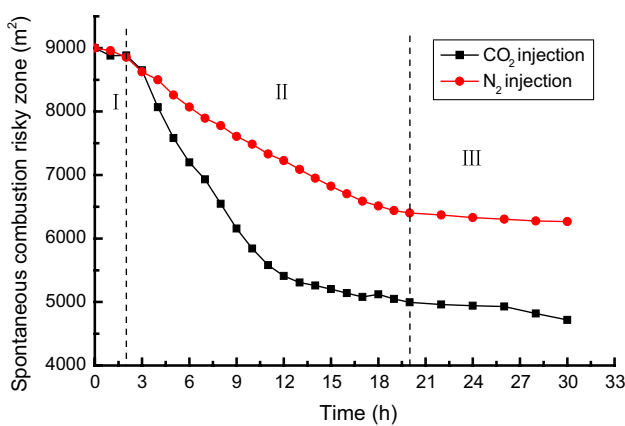


Fig. 11 Reduction of spontaneous combustion dangerous zone with CO₂ or N₂ injection

the workface. These positions are far from the workface and the air leakage speed is lower, which reduces the loss of inert gas. The inert gas seeps into the goaf and decreases the oxygen concentration. So O₂ concentration drops to less than the critical oxygen concentration or even <1 %. The inert gas dilutes the oxygen concentration significantly and decreases the area of the spontaneous combustion dangerous area. That is to say, the injection locations of 36 and 60 m behind the workface have higher inerting effect. Comparing between CO₂ and N₂ injection, the influence scope of oxidation zone is smaller with N₂ nitrogen at same location.

Comparisons of O₂ distributions at different measuring pipelines simulated with/without inert gas injection are

presented in Fig. 14. The distance that the oxygen concentration decreases down to 5 % with N₂ injection is about 48–80 m behind the workface; while it is about 10–80 m with CO₂ injection, which is about 2.2 times more than the nitrogen injection. Meanwhile, the effecting distance with CO₂ injection is about 66.7 m in the tendency direction, and it is <33.3 m with N₂ injection. The influencing scope with CO₂ injection is deeper. CO₂ dilutes oxygen in the zone between workface and injecting port. N₂ injection only decreases the oxygen concentration in the zone around the injecting port.

Figure 15 compares the areas of the spontaneous combustion dangerous zone and the asphyxia zone with CO₂ or N₂ injection. The area that oxygen concentration decreases to below 5 % with CO₂ injection for 20 h is about 1.25–2.4 times larger than that with N₂ injection. The area of the combustion spontaneous zone when the injecting CO₂ port is located at the return-side is about 1.14–1.18 times larger than that located at the intake-side. And it is about 1.06–1.13 times with N₂ injection. Since the ventilation pressure can hinder the seepage of carbon dioxide and nitrogen, injecting inert gas on the intake-side is better than on the return-side. Meanwhile, the area of the combustion spontaneous dangerous zone when the inert gas entrance is 60 m behind the workface on the intake-side is 1.10 and 1.26 times than those 36 m behind the workface. It seems that the inerting effect is better when the injection entrance is 60 m behind the workface.

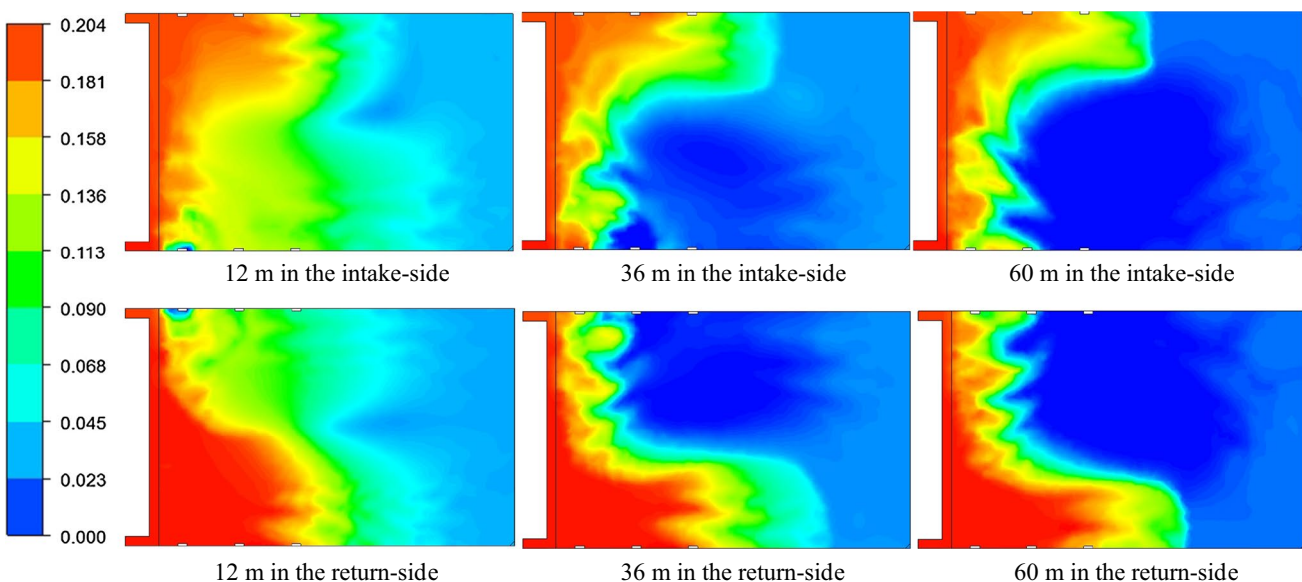


Fig. 12 Comparison of O₂ distributions at the floor level with different CO₂ injection locations: 12, 36 or 60 m behind workface on the intake-side or return-side

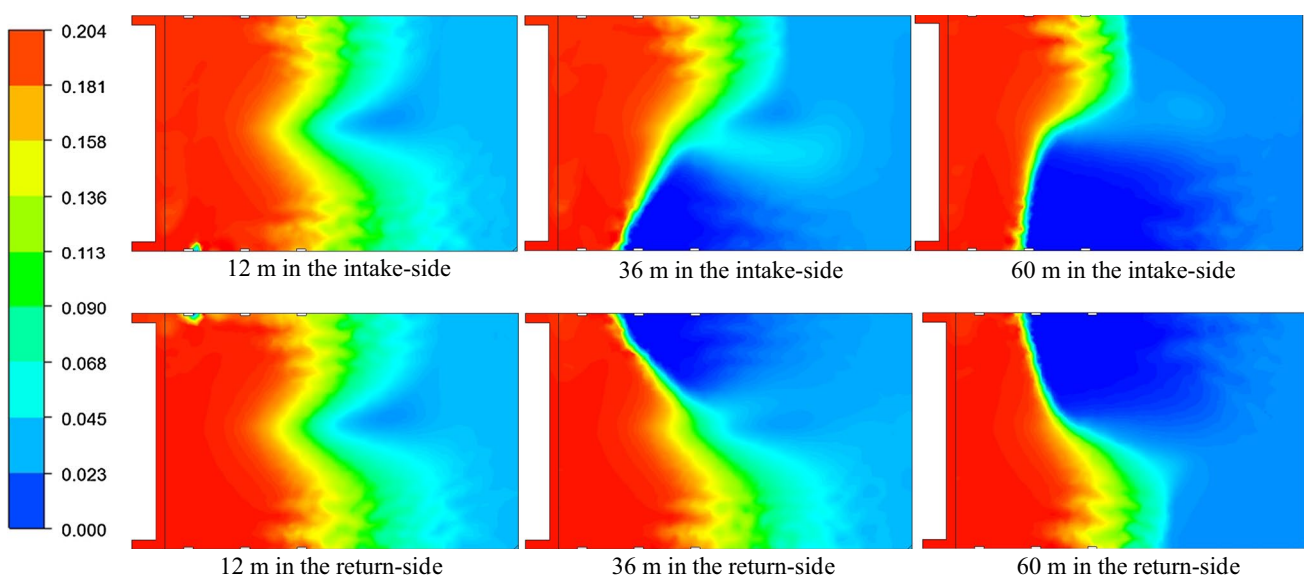


Fig. 13 Comparison of O₂ distributions at the floor level with different N₂ injection locations: 12, 36 or 60 m behind workface on the intake-side or return-side

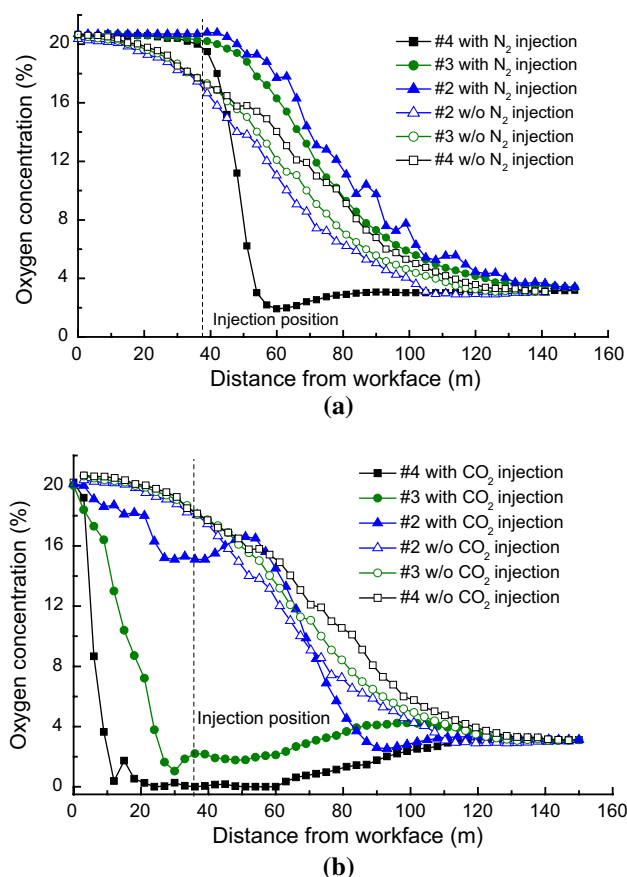


Fig. 14 Comparison of O₂ distributions along three measuring pipelines simulated with and without inert gas injection

5 Conclusions

This paper proposed a new 3-D porous model for mine goaf based on stress status. Simulations based on this model were carried out and compared with field experiment in the case without inert gas injection. The numerical results are in good consistency with the experimental data. This validated the porous model as well as the numerical coding.

The focus of this study is the numerical investigation of the effects of inert gas injection. The results demonstrated the accumulation mechanism of injected inert gas CO₂ or N₂. It is found that CO₂ gas accumulates at the ground level of the goaf because of gravity. On the other side, a large portion of N₂ gas seeps up in the goaf and moves to a zone near the workface. The results also show that the evolution of the spontaneous combustion dangerous zone during inert gas injection could be classified into three phases: the slow inserting phase, in which the dangerous zone decreases slowly and shows the level change with time; the rapid accelerating phase, in which the rate of the area of the dangerous zone with carbon dioxide injection shows a negative exponential relationship with time, while it shows a negative linear relationship with nitrogen injection; and the stable inserting phase, in which the spontaneous combustion dangerous zone decreases slowly or keeps steady.

The study shows that the effect on reducing O₂ concentration via injecting CO₂ is better than N₂ injection. The distance, which is about 66.7 m at the tendency, that the oxygen concentration is decreased down to below 5 % with

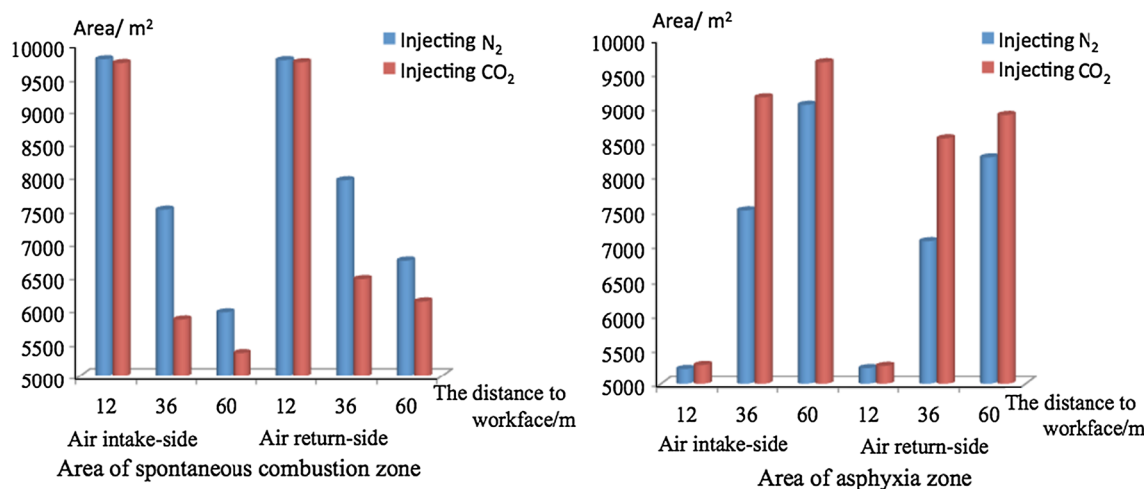


Fig. 15 Comparisons of the spontaneous combustion and asphyxia zones with inert gas injection at different locations

CO₂ injection is about twice that of N₂ injection. And the area of the asphyxia zone after injecting CO₂ 20 h is about 1.25–2.4 times larger than N₂ injection.

Through this study, a better inert gas injection location in the goaf is suggested at the oxidation zone or the transitional zone between the heat dissipation zone and oxidation zone. The optimal time of injecting inert gas is the time of the slow inerting phase and rapid accelerating inerting phase. The area of the combustion spontaneous zone when the injection is located in the return airway is about 1.06–1.18 times larger than that located on the intake-side of the goaf.

In future studies, temperature-dependence of properties and more complicated chemical reactions in combination with the energy equation should be taken into account to study more complicated situations in coal spontaneous combustion.

Acknowledgments This research was supported by the National Natural Science Foundation of China (Grant Nos. 51104154 and 51134020), Central Subordinate University Basic Scientific Research Foundation (2011QNA05) and CUMT Innovation and Entrepreneurship Fund for Undergraduates (201403 and 201503).

References

- 1. Krishnaswamy S, Agarwal PK, Gunn RD (1996) Low-temperature oxidation of coal. 3. Modeling spontaneous combustion in coal stockpiles. *Fuel* 75:353–362
- 2. Li X (1998) Coal mine safety in China. China Coal Industry Press, Beijing
- 3. Hofgren H, Sundén B (2015) Evaluation of Planck mean coefficients for particle radiative properties in combustion environments. *Heat Mass Transf* 51:507–519
- 4. Achim D, Naser J, Morsi YS, Pascoe S (2009) Numerical investigation of full scale coal combustion model of tangentially fired boiler with the effect of mill ducting. *Heat Mass Transf* 46:1–13
- 5. Wang H, Dlugogorski BZ, Kennedy EM (2003) Coal oxidation at low temperatures: oxygen consumption, oxidation products, reaction mechanism and kinetic modeling. *Prog Energy Combust Sci* 29:487–513
- 6. Deng J, Xu J, Li L (2001) Experimental investigation on the relationship of oxygen consumption rate of coal and the concentration of oxygen. *J Xiangtan Min Inst* 3:12–18
- 7. Singh D, Croiset E, Douglas PL, Douglas MA (2003) Techno-economic study of CO₂ capture from an existing coal-fired power plant: MEA scrubbing vs. O₂/CO₂ recycle combustion. *Energy Convers Manag* 44:3073–3091
- 8. Shao H, Jiang S, Wu Z (2013) Numerical simulation on fire prevention by infusing carbon dioxide into goaf. *J Min Saf Eng* 30(1):154–158
- 9. Li X (2003) Numerical simulation and parameter determination of nitrogen injection process in Fire prevention and Extinguishing in fully mechanized longwall top-coal goaf. *China Saf Sci J* 5:57–61
- 10. Zhang Y, Liu P, Li P, Huang Z, Gao Y (2013) Research on influence of injecting CO₂ at goaf of 13304 caving face of Sunjiaogou coal mine on its three zones of spontaneous combustion. *Disaster Adv* 6:341–349
- 11. Sun Y, Ma J (2015) Application of collocation spectral method for irregular convective–radiative fins with temperature-dependent internal heat generation and thermal properties. *Int J Thermophys* 36(10–11):3133–3152
- 12. Liang Y, Zhang T, Wang S, Sun J (2012) Heterogeneous model of porosity in gob and its airflow field distribution. *J China Coal Soc* 09:1203–1207
- 13. Che Q (2010) Study on coupling law of mixed gas three-dimensional multi-field in goaf. *China Univ Min Technol, Beijing*
- 14. Yuan L, Smith AC (2009) CFD modeling of spontaneous heating in a large-scale coal chamber. *J Loss Prev Process Ind* 22(4):426–433
- 15. Wang F (2004) Computational fluid dynamics: the basics with application. Tsinghua University Press, Beijing
- 16. Qian M, Li H (1982) A study of the behaviour of overlying strata in longwall mining and its application to strata control. *J China Coal Soc* 7(2):1–12
- 17. Hoek E, Bray JW (1981) Rock slope engineering, revised, 3rd edn. Institution of Mining and Metallurgy, London

18. Creedy DP (1993) Methane emissions from coal related sources in Britain : development of a methodology. *Energy Ind Source* 26(1):419–439
19. Li Z, Yi G, Wu J, Guo D, Zhao C (2012) Study on spontaneous combustion distribution of goaf based on the “O” type risked falling and non-uniform oxygen. *J China Coal Soc* 3:484–489
20. Creedy DP, Clarke RDC (1992) Minimizing firedamp risks on high production coalfaces: a computational modelling approach. In: Proceedings of the international symposium: safety, hygiene and health in mining, pp 192–203
21. Ren T (1997) CFD modeling of methane flow around longwall coal faces. In: Proceedings of the 6th int mine ventilation congress, pp 17–22
22. Ren T, Edwards JS (2000) Three-dimensional computational fluid dynamics modeling of methane flow through permeable strata around a longwall face. *Min Technol* 109(1):41–48
23. ANSYS Fluent Tutorial Guide (2013). <http://148.204.81.206/Ansys/150/ANSYS%20Fluent%20Tutorial%20Guide.pdf>
24. Zhu H, Wang H, He C, Yang C (2013) Experimental of effect of oxygen concentration to coal low-temperature oxidation kinetics parameters. *J Liaoning Tech Univ (Natural Science)* 32:1153–1156
25. Wang D (2008) Mine fires. China University of Mining and Technology Press, Xuzhou